Supporting information

Multisite synergistic-modulating elementary steps for efficient alkaline hydrogen evolution via NiCu/NiMoO$_x$ nanocomposites

Haiyao Li[1], Zhimin Li[2], Zhishan Li[2], Zhengfu Zhang[1], Chengping Li[1], and Jinsong Wang[1*]*

[1]Faculty of Materials Science and Engineering, Kunming University of Science and Technology 650093 Kunming, P. R. China

[2]Faculty of Metallurgical and Energy Engineering, Kunming University of Science and Technology, 650093 Kunming, P. R. China

*Corresponding authors

E-mail *addresses*: jswang512@kust.edu.cn (Jinsong Wang)

zhimin_li015@126.com (Zhimin Li)

Experimental Section

Electrochemical measurements. All electrochemical measurements were conducted by CHI760E electrochemical workstation. The samples were employed as the working electrode, a graphite electrode was used as the counter electrode and a saturated Ag/AgCl was utilized as the reference electrode. The electrochemical impedance spectroscopy (EIS) was measured at a voltage of -1.1 V with the frequency range of 100 kHz-0.01 Hz. To evaluate HER activity, the linear sweep voltammetry (LSV) curves were recorded at potential range from -1.0 to -1.5 V vs. Ag/AgCl with a scan rate of 2 mV s^{-1}. The potential was converted to reversible hydrogen electrode (RHE) by the equation of $E_{RHE} = E_{Ag/AgCl} + 0.198 + 0.0591\times pH$. The electrochemical active surface area (ECSA) was estimated

according to the double layered capacitance (C_{dl}). The cyclic voltammetry (CV) were tested at different scan rates (2 mV s^{-1}, 4 mV s^{-1}, 6 mV s^{-1}, 8 mV s^{-1}, and 10 mV s^{-1}) in a non-Faradaic region (-0.85 to -0.95V *vs.* Ag/AgCl), and plotting the difference in current density between the anodic and cathodic sweeps ($\Delta j = j_a - j_c$) at 0.9V *vs.* Ag/AgCl as a function of scan rates yielded a straight line with slope equal to C_{dl}.

The ECSA of as-synthesized catalysts is calculated following:

$$\mathrm{ECSA} = \frac{C_{\mathrm{dl}}(mF \cdot cm^{-2})}{C_{\mathrm{s}} \times uF \cdot cm^{-2} percm^{2}_{ECSA}}$$

where the specific capacitance for a flat surface (C_S) is generally between 0.02-0.06 mF cm^{-2}. Therefore, we used C_S of 0.04 mF cm^{-2} to calculate the ECSA.

The TOF value is calculated from the equation:

$$\mathrm{TOF} = \frac{I}{2 * NF}$$

where *I* is the measured current during the linear sweep measurement, *N* is number of the active sites, and *F* is the Faraday constant (96485 C mol^{-1}). Assuming a one electron redox and oxidation process, the upper limit of active sites could be calculated by the follow equation: $N = \frac{Q}{2 * F}$, cyclic voltammetry were measurements from -0.85 to -0.95 V *vs.* Ag/AgCl at 2 mV s^{-1} in 1 M KOH solution, where *Q* is the whole charge of CV curve.

DFT Calculations. DFT calculations were performed using the Vienna Ab Initio Simulation Package (VASP).[1-3] The electron ion interaction was described with the projector augmented wave (PAW) method.[4] The electron exchange and correlation energy were treated within the generalized gradient approximation (GGA) in the Perdew-Burke-Ernzerhof formalism (PBE).[5, 6] The energy cut-off for the plane-wave basis was set to 500 eV for all calculations. Conjugated gradient method was used to the geometry optimization and all the atomic coordinates were fully relaxed until the maximal force

on each atom was less than 0.05 eV/Å, and the convergence condition for energy is 10^{-4} eV. All constructions possess larger than 20 Å vacuum region in the z direction to minimize the interaction between planes. The Monkhorst Pack [7] sampling scheme were set of 2×2×1 and 4×4×1 for geometry optimization, electronic self-consistent calculation, respectively. The ΔG_H is calculated following:

$$\Delta G_H = \Delta E_H + \Delta E_{ZPE} - T\Delta S_H$$

Where ΔE_H is the binding energy of hydrogen atom, and ΔE_{ZPE} and $T\Delta S_H$ is zero-point energy corrections and the entropic corrections, respectively, which can be simplified as 0.24 eV.

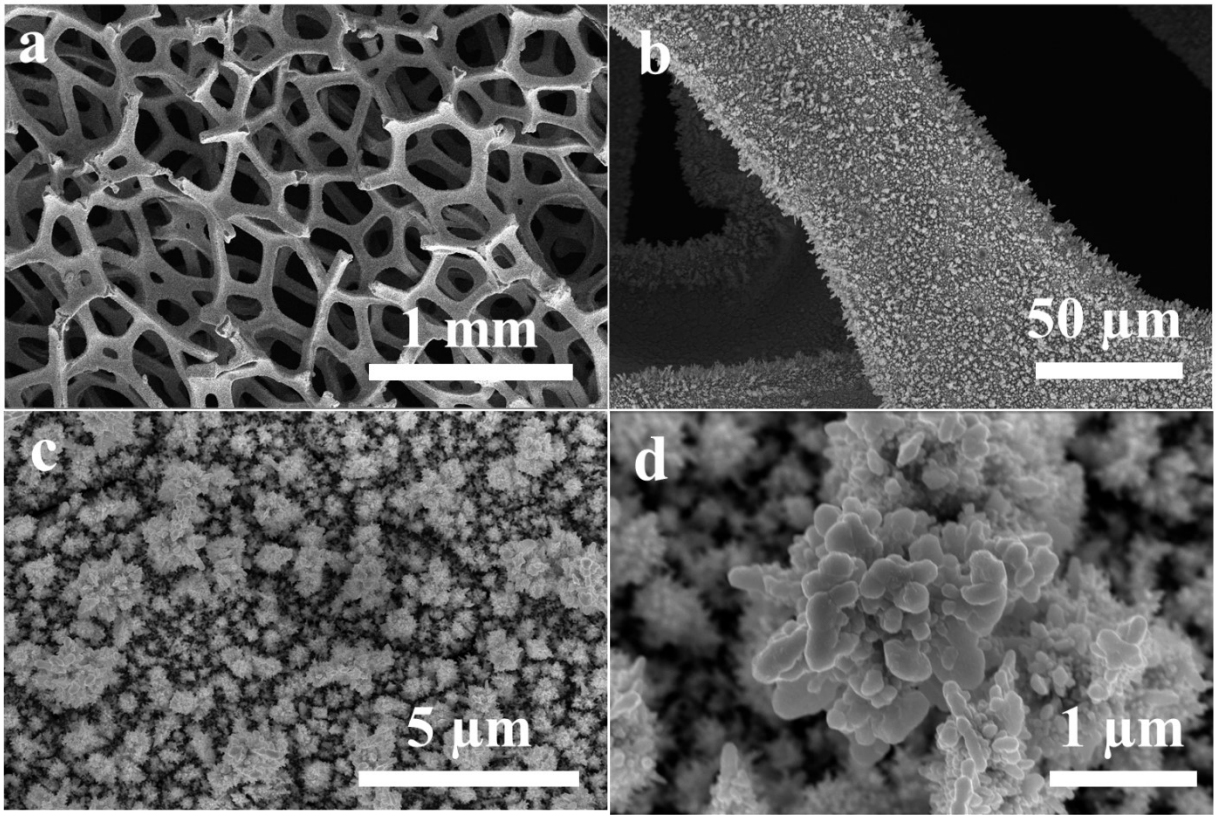

Figure S1. The FE-SEM images of NiCu with different magnifications.

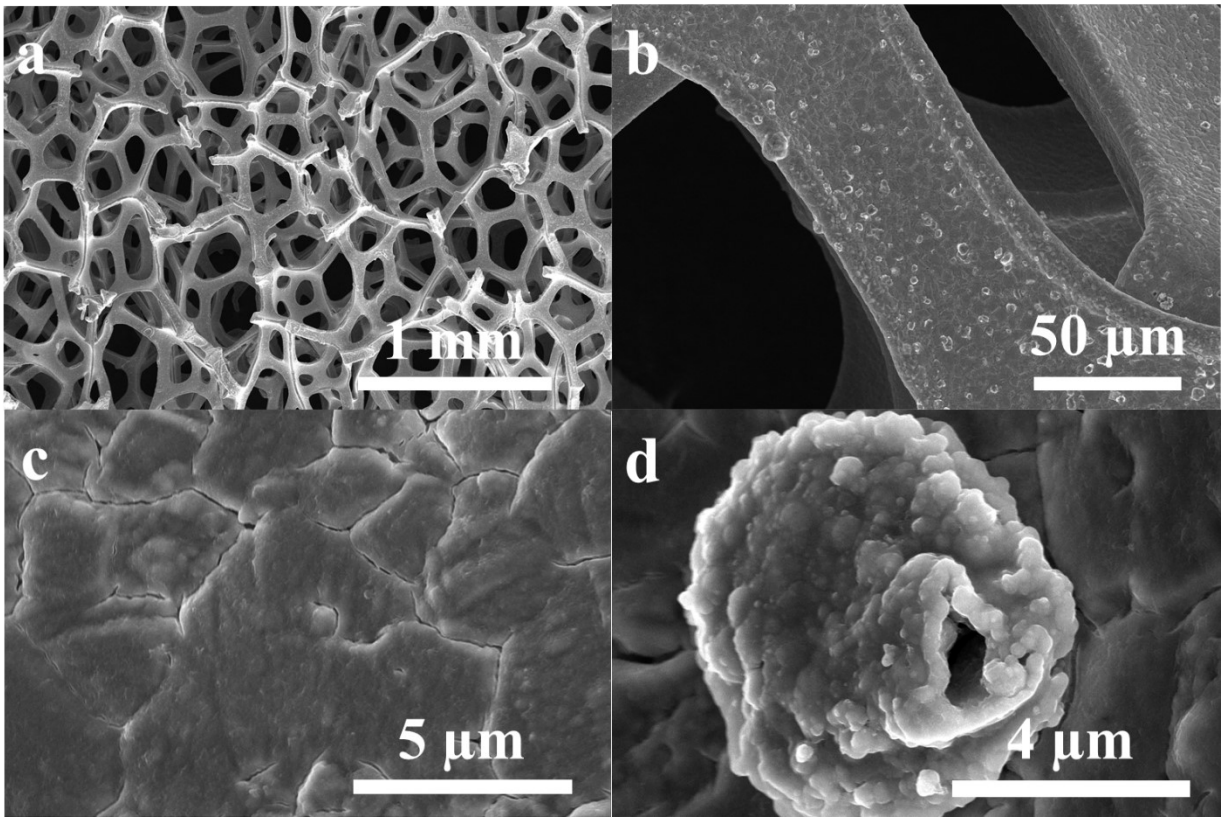

Figure S2. The FE-SEM images of NiMo with different magnifications.

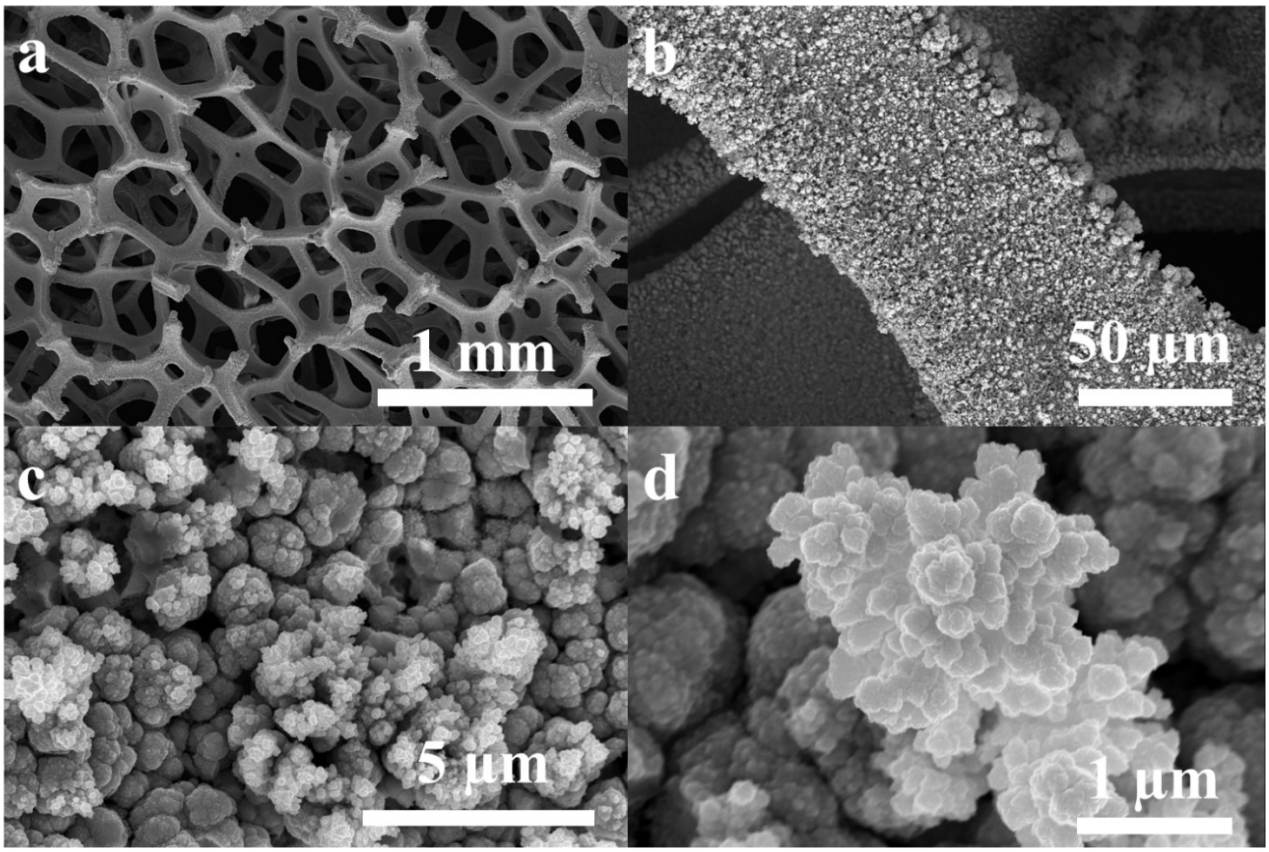

Figure S3. The FE-SEM images of NiCu/MoO_x with different magnifications.

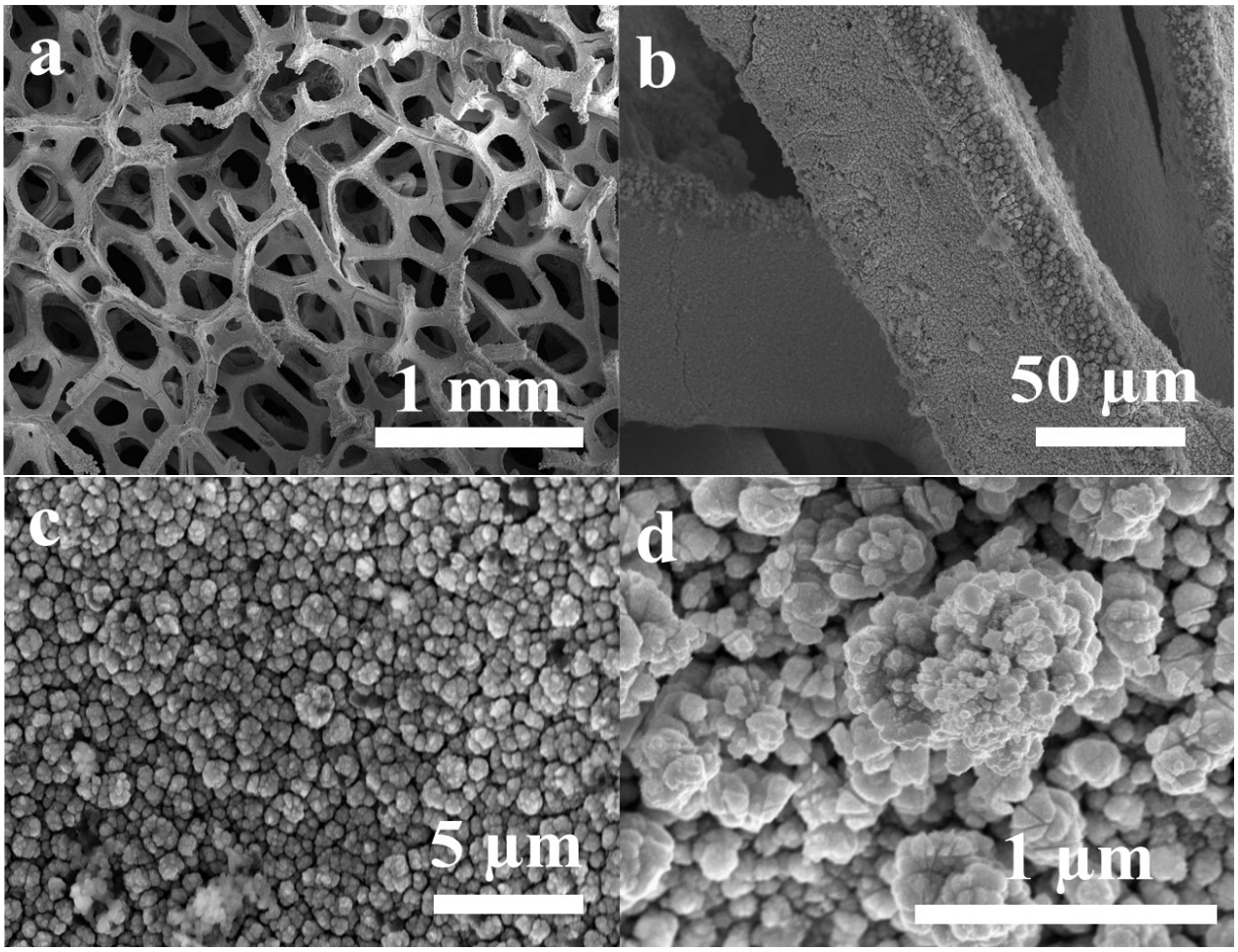

Figure S4. The FE-SEM images of NiCu/MoO_x after 65 h at 10 mA cm^{-2} in 1M KOH.

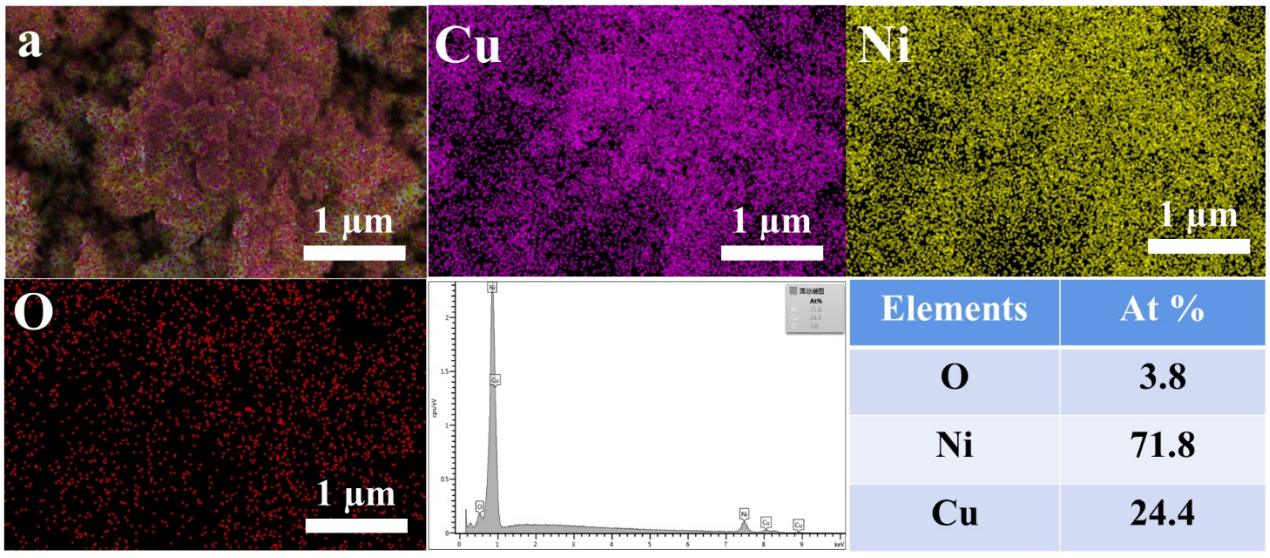

Elements	At %
O	3.8
Ni	71.8
Cu	24.4

Figure S5. The SEM image of NiCu with EDX elemental mapping and corresponding element amounts.

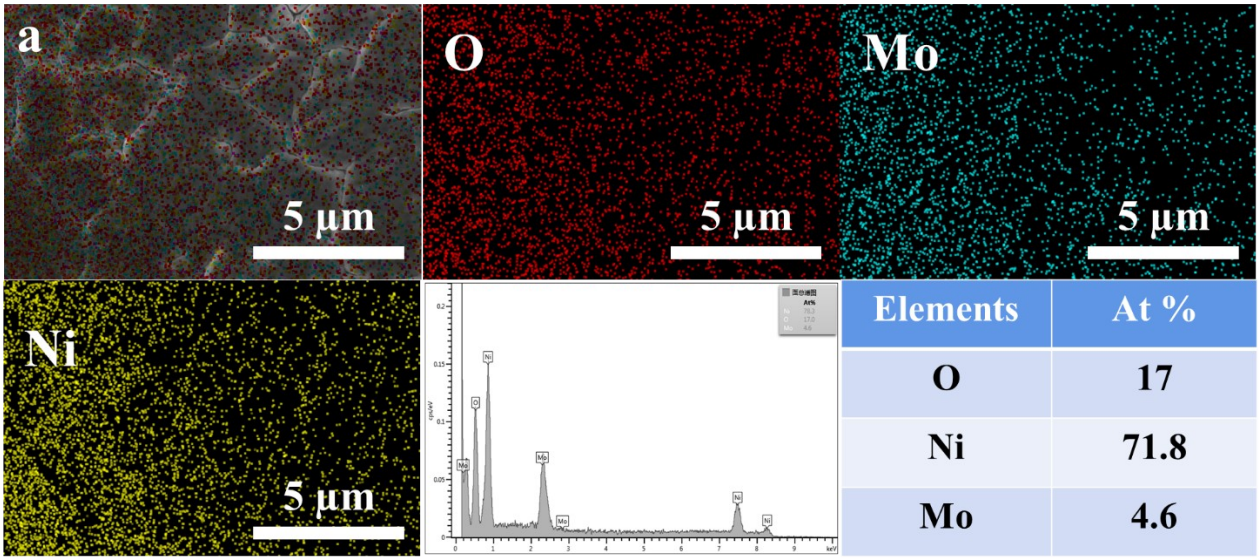

Figure S6. The SEM image of Ni/MoO_x with EDX elemental mapping and corresponding element amounts.

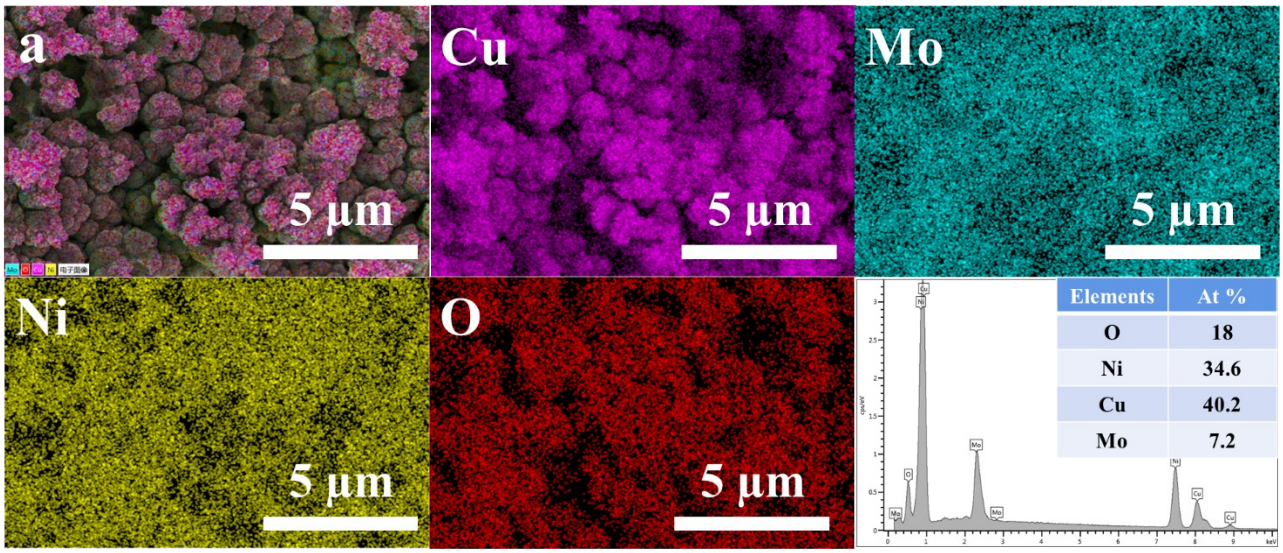

Figure S7. The SEM image of NiCu/MoO_x with EDX elemental mapping and corresponding element amounts.

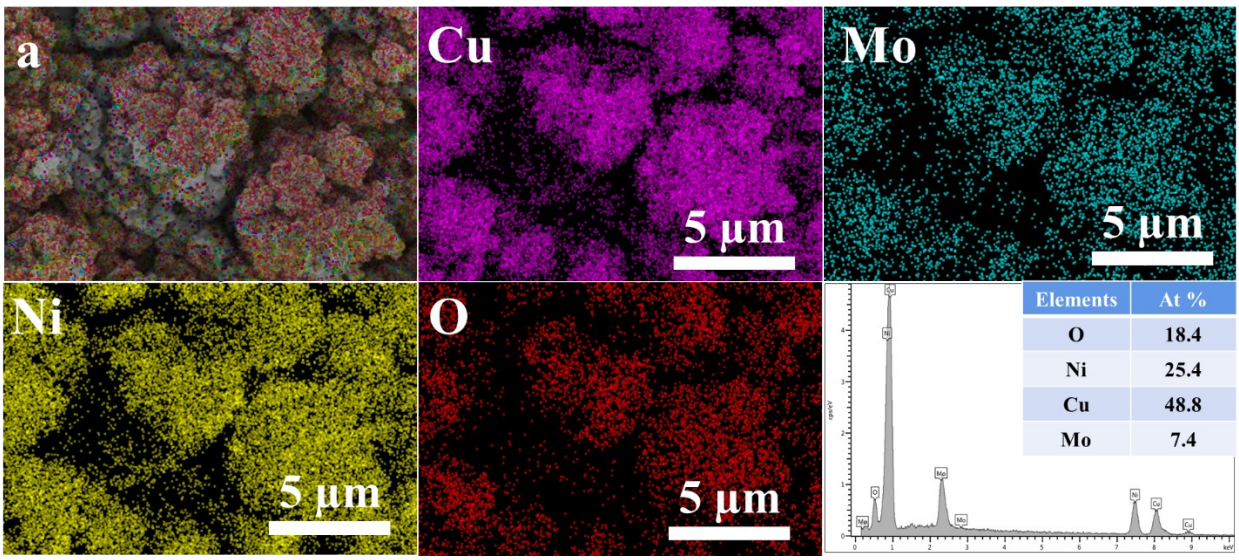

Figure S8. The SEM image with EDX elemental mapping and corresponding element amounts of $NiCu/MoO_x$ after stability test.

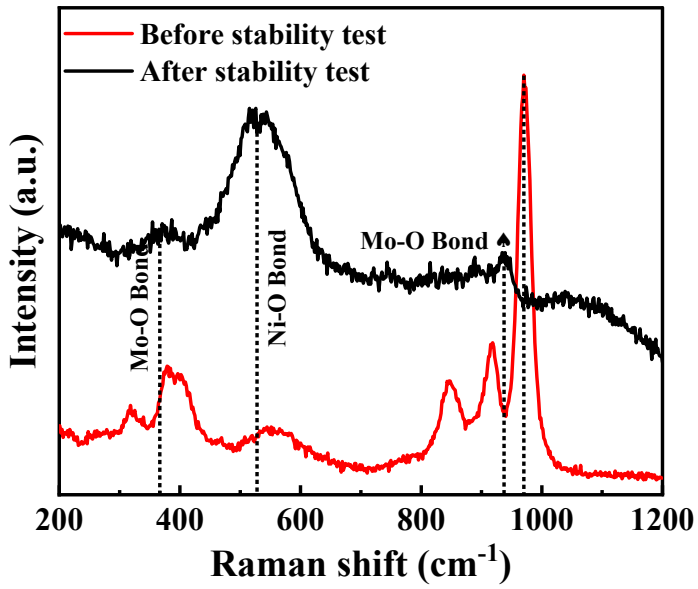

Figure S9. The Raman spectra of $NiCu/MoO_x$ before and after stability test.

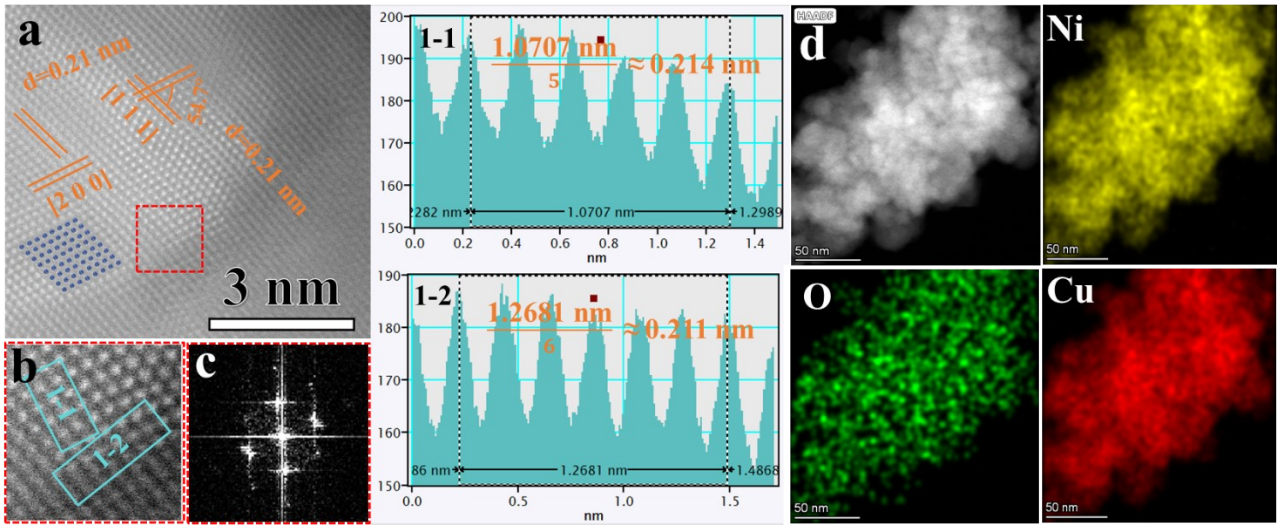

Figure S10. The HAADF-STEM of NiCu.

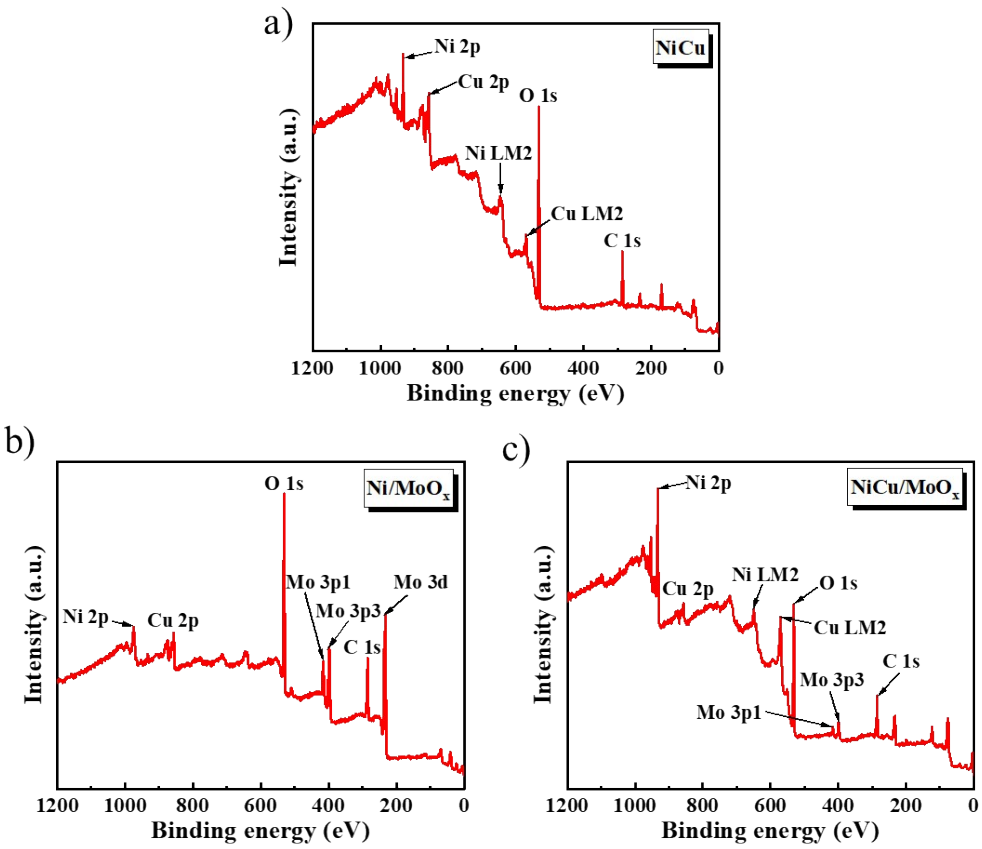

Figure S11. The XPS survey of (a) NiCu, (b) Ni/MoO_x and (c) NiCu/MoO_x.

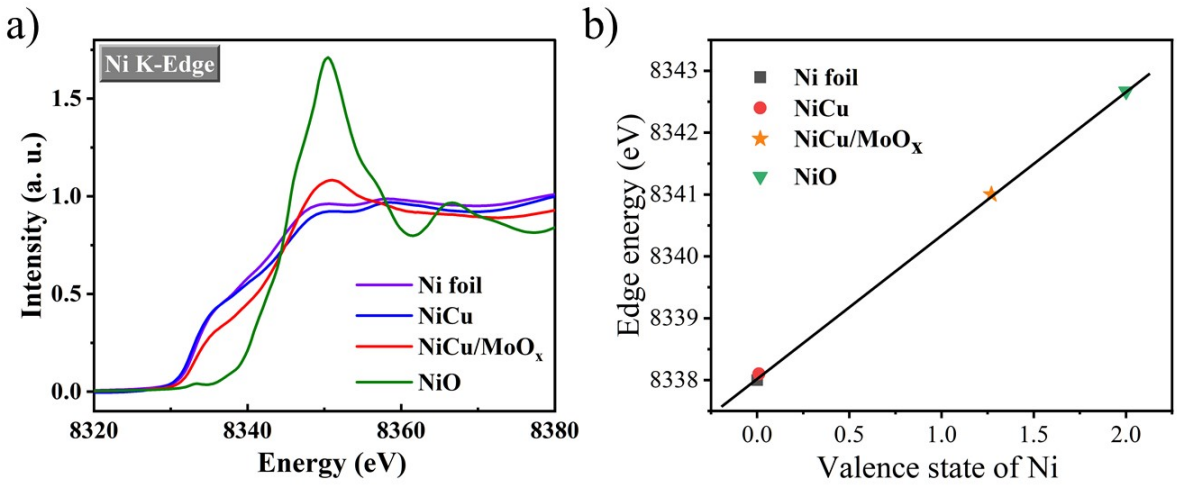

Figure S12. a) Ni K-edge XANES of NiCu, NiCu/MoO_x, Ni foil and NiO; b) Corresponding accurate Ni value.

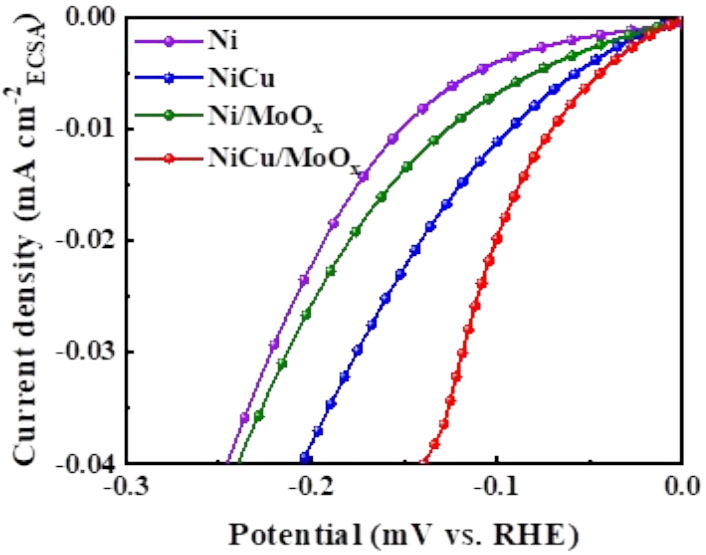

Figure S13. The ECSA-normalized LSV curves of the prepared Ni, NiCu, Ni/MoO_x and NiCu/MoO_x toward HER in 1M KOH.

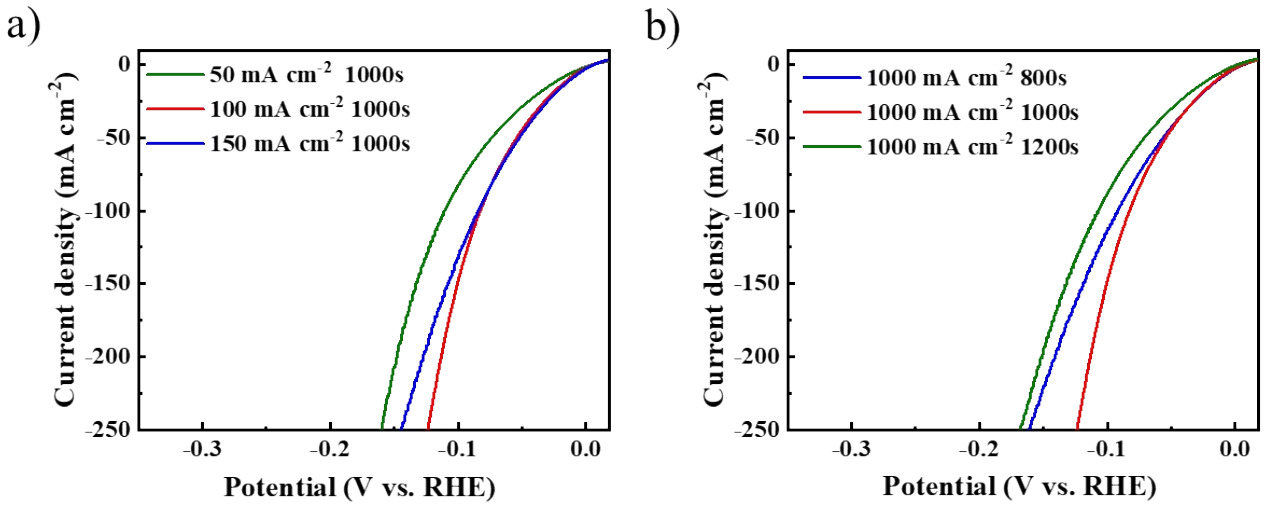

Figure S14. The LSV curves of $NiCu/MoO_x$ with different deposition currents and times for HER in 1M KOH.

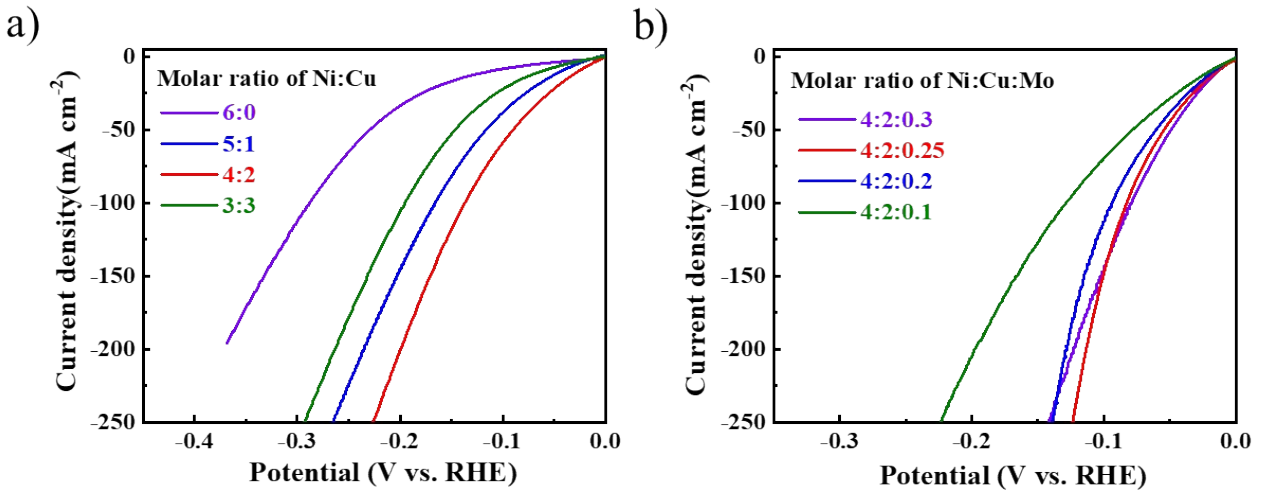

Figure S15. The LSV curves of different ratios of a) Ni/Cu and b) Ni/Cu/Mo toward HER with scan rates of 2 mV S^{-1} in 1M KOH.

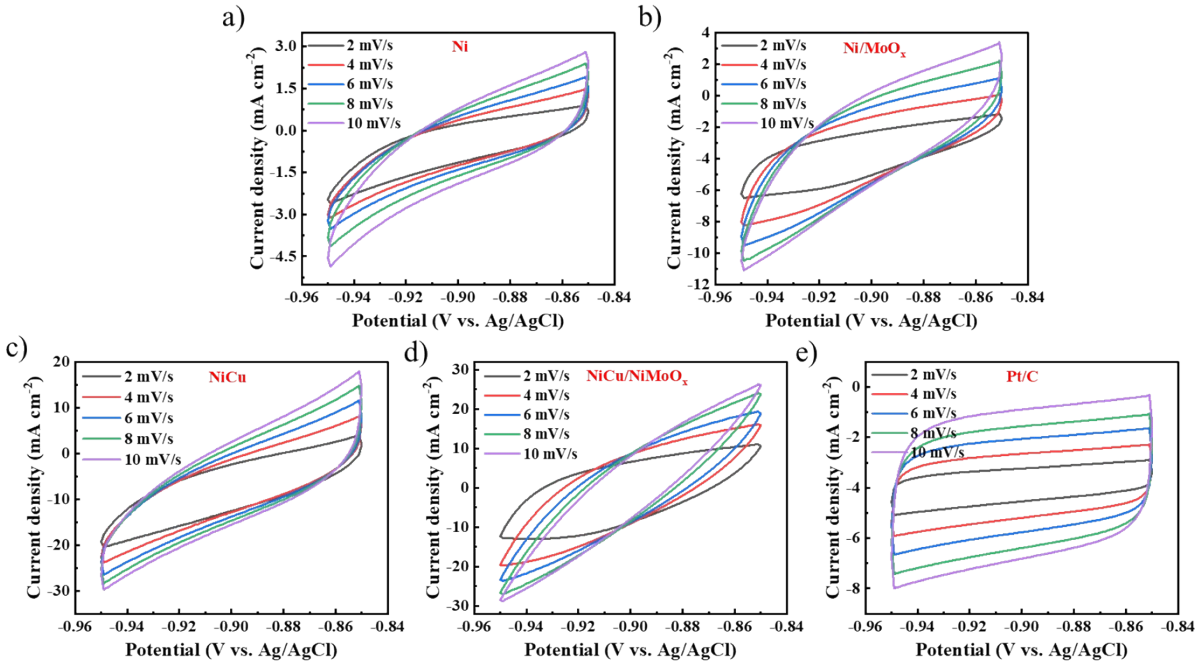

Figure S16. The cyclic voltammograms (CV) of (a) Ni, (b) Ni/MoO_x, (c) NiCu, (d)NiCu/MoO_x, (e) Pt/C with scan rates of 2-10 mV S^{-1} in 1M KOH.

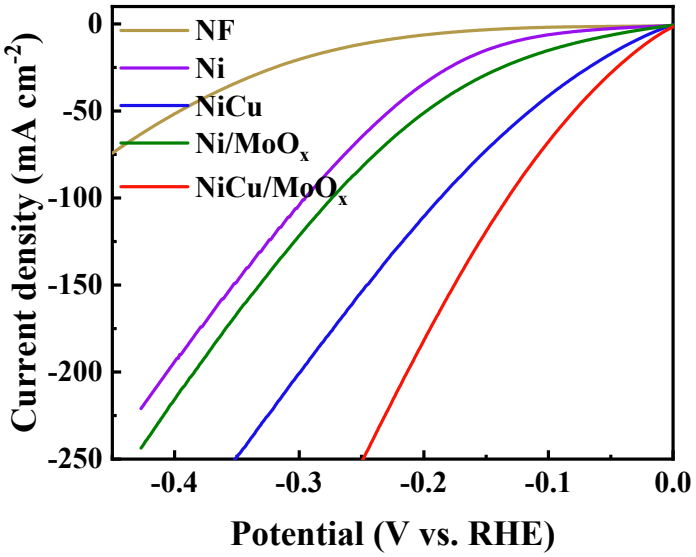

Figure S17. The LSV curves of the prepared NF, Ni, Ni/MoO_x, NiCu, NiCu/MoO_x without IR compensation with scan rates of 2 mV S^{-1} in 1M KOH.

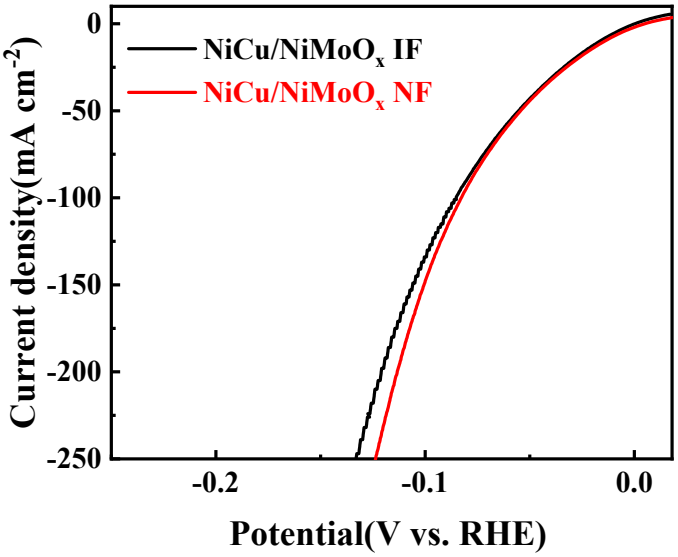

Figure S18. The LSV curves of loading NiCu/MoO$_x$ catalysts onto different substrates (nickel foam and iron foam).

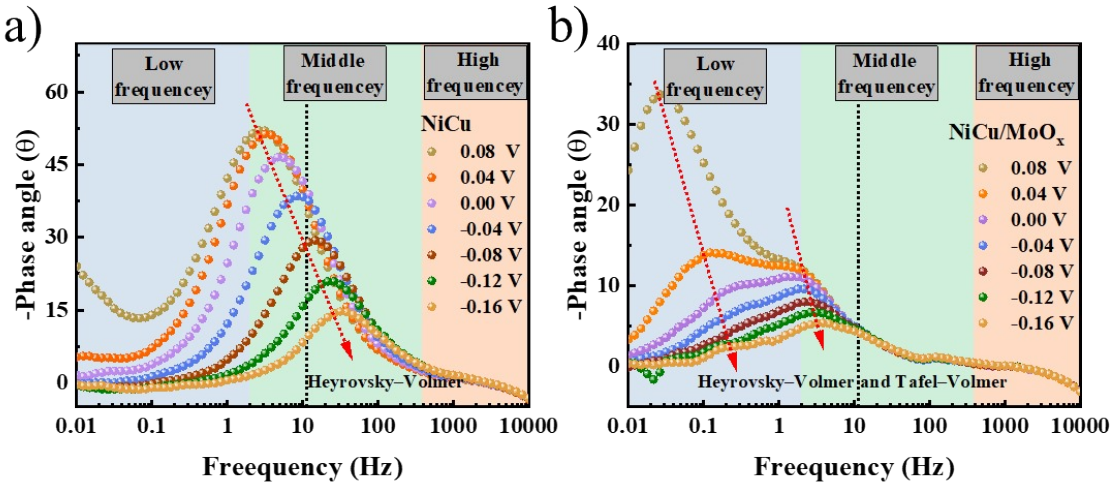

Figure S19. Bode plots for a) NiCu in 1 M KOH with Heyrovsky step as RDS, and b) NiCu/MoO$_x$ with mixture mechanisms (Heyrovsky–Volmer and Tafel–Volmer).

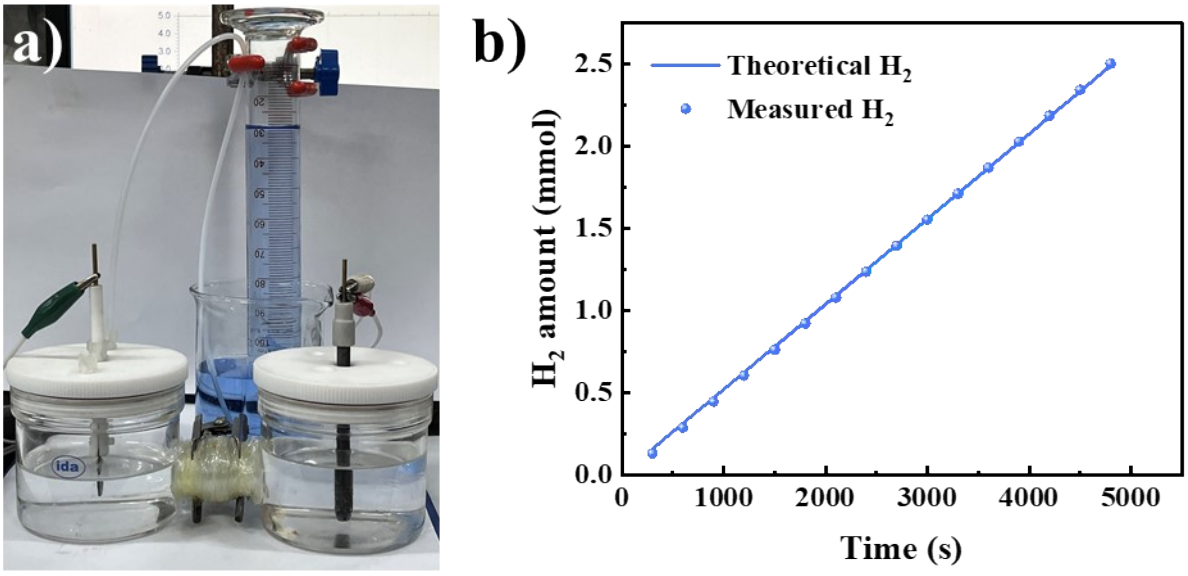

Figure S20. a) Physical picture of the device, b) The amount of H_2 collected by the water drainage method as a function of time for $NiCu/MoO_x$ under a constant current density of 100 mA cm^{-2}.

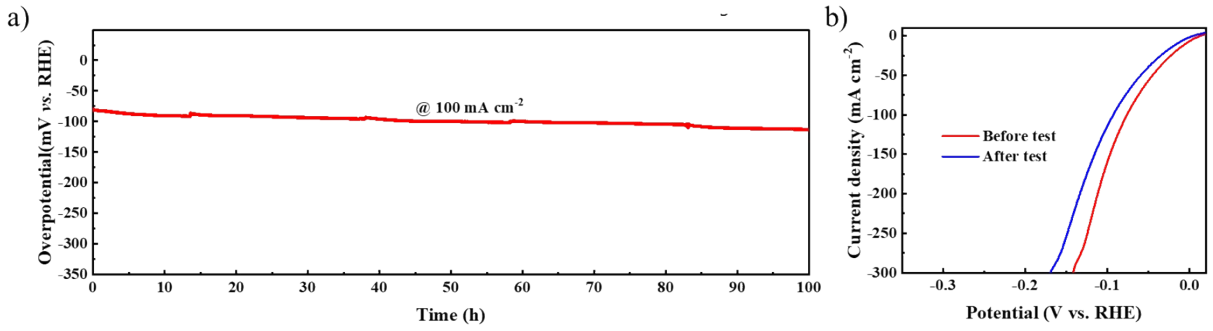

Figure S21. a) a) The chronopotentiometry (i-t) tests of the $NiCu/MoO_x$ electrode at 100 mA cm^{-2}. b) The lsv before and after test.

Table S1. Ni, Cu and Mo atomic percentages obtained from ICP-OES results.

Samples	Chemical composition (mg/L)		
	Ni	Cu	Mo
NiCu	1.26	1.49	/
Ni/MoO_x	1.23	/	0.46
$NiCu/MoO_x$	1.41	0.96	0.92

Table S2. Comparison of HER performance for $NiCu/MoO_x$ with other reported electrocatalysts in 1 M KOH.

Catalysts	Electrolyte	η(mV) j=-10 $mAcm^{-2}$	Tafel slope ($mV\ dec^{-1}$)	References
$NiCu/MoO_x$	1.0M KOH	14	38.3	this work
Pt/MgO	1.0M KOH	39	39	Nat. Commun. 2022. 13. 2024[8]
$V\text{-}Ni_2MoN_3$	1.0M KOH	54	42.8	Electrochimica Acta 337(2020)135689[9]
NiCo LDH/NF	1.0M KOH	51	70	Adv. Funct. Mater. 28(2018)1704594[10]
Mo-NiO/Ni	1.0M KOH	50	86	ACS Energy Lett. 2019,4,3002-3010[11]
Sr_2RuO_4	1.0M KOH	61	51	Nat. Commun. 2019, 10, 149[12]
$P\text{-}Mo\text{-}Ni(OH)_2$	1.0M KOH	22	80	Appl. Catal. B-Environ. 260(2020)118154[13]
$Ni_3N\text{-}V_2O_3$	1.0M KOH	57	50	Appl. Catal. B-Environ. (2020).119590[14]
$Ru/Ni(OH)_2/NF$	1.0M KOH	25	45	J. Mater. Chem. A 2019,7, 11062-11068[15]
Pt/NiRu-OH	1.0M KOH	38	39	Appl. Catal. B-Environ. 2020, 269, 118824[16]
$Ni_5P_4\text{-}Ru/CC$	1.0M KOH	54	52	Adv. Mater: 2020, 32, 1906972[17]
RuCo@N-C	1.0M KOH	28	31	Nat. Commun. 2017, 8, 14969[18]
Ru@SC-CDs	1.0M KOH	29	57	Nano Energy 2019, 65, 104023[19]
NiFeRu-LDH	1.0M KOH	29	31	Adv. Mater 2018, 30,

				1706279[20]
Ru@NG-750	1.0M KOH	40	35.9	ACS Catal. 2019, 9, 9897-9904[21]
$Pt/Co(OH)_2$	1.0M KOH	32	70	ACS Catal. 2017, 7, 7131-7135[22]
Vs-Co_3S_4@NF	1.0M KOH	46	66	Appl. Catal. B-Environ. 322(2023)122104[23]
ReS_2/NiS	1.0M KOH	78	76	Chemical Engineering Journal 451(2023)138905[24]
Ni(Cu)/NF	1M KOH	27	33.3	Small 2018, 14, 1704137[25]
Pt_{SA}M-NiO/Ni	1M KOH	26	27.07	Nat Commun 12, 3783 (2021).[26]

Reference

[1] P. Hohenberg, W. Kohn, Inhomogeneous Electron Gas, Physical Review 136(3B) (1964) B864-B871. https://doi.org/10.1103/PhysRev.136.B864.

[2] W. Kohn, L.J. Sham, Self-Consistent Equations Including Exchange and Correlation Effects, Physical Review 140(4A) (1965) A1133-A1138. https://doi.org/10.1103/PhysRev.140.A1133.

[3] G. Kresse, J. Hafner, Ab initio molecular dynamics for liquid metals, Physical Review B 47(1) (1993) 558-561. https://doi.org/10.1103/PhysRevB.47.558.

[4] P.E. Blöchl, Projector augmented-wave method, Physical Review B 50(24) (1994) 17953-17979. https://doi.org/10.1103/PhysRevB.50.17953.

[5] J.P. Perdew, K. Burke, M. Ernzerhof, Generalized Gradient Approximation Made Simple, Physical Review Letters 77(18) (1996) 3865-3868. https://doi.org/10.1103/PhysRevLett.77.3865.

[6] G. Kresse, J. Furthmüller, Efficient iterative schemes for ab initio total-energy calculations using a plane-wave basis set, Physical Review B 54(16) (1996) 11169-11186. https://doi.org/10.1103/PhysRevB.54.11169.

[7] H.J. Monkhorst, J.D.J.P.r.B. Pack, Special points for Brillouin-zone integrations, 13(12) (1976) 5188.

[8] H. Tan, B. Tang, Y. Lu, Q. Ji, L. Lv, H. Duan, N. Li, Y. Wang, F. Sihua, Z. Li, C. Wang, F. Hu, Z. Sun, W. Yan, Engineering a local acid-like environment in alkaline medium for efficient hydrogen evolution reaction, Nature Communications 13 (2022) 2024. https://doi.org/10.1038/s41467-022-29710-w.

[9] P. Zhou, X. Lv, Y. Gao, Z. Liang, Y. Liu, Z. Wang, P. Wang, Z. Zheng, Y. Dai, B. Huang, Synthesis of novel cubic Ni2Mo3N and its electronic structure regulation by vanadium doping towards high-efficient HER electrocatalyst, Electrochimica Acta 337 (2020) 135689. https://doi.org/10.1016/j.electacta.2020.135689.

[10] T. Tang, W.-J. Jiang, S. Niu, N. Liu, L. Hao, Q. Zhang, W. Wen, Y.-Y. Chen, L. Huang, F. Gao, J.-S. Hu, Kinetically Controlled Coprecipitation for General Fast Synthesis of Sandwiched Metal Hydroxide Nanosheets/Graphene Composites toward Efficient Water Splitting, Advanced Functional Materials 28 (2018). https://doi.org/10.1002/adfm.201704594.

[11] J. Huang, J.C. Han, W. Tao, K. Feng, T. Yao, X.-J. Wang, S. Liu, J. Zhong, z. zhang, Y. Zhang, Boosting the Hydrogen Transfer during Volmer Reaction at Oxides/metal Nanocomposites for Efficient Alkaline Hydrogen Evolution, ACS Energy Letters XXXX (2019). https://doi.org/10.1021/acsenergylett.9b02359.

[12] Y. Zhu, H. Tahini, Z. Hu, J. Dai, Y. Chen, H. Sun, W. Zhou, M. Liu, S. Smith, H. Wang, Z. Shao, Unusual synergistic effect in layered Ruddlesden−Popper oxide enables ultrafast hydrogen evolution, Nature Communications 10 (2019). https://doi.org/10.1038/s41467-018-08117-6.

[13] W. Zhang, T. Yuanhao, L. Yu, X.-Y. Yu, Activating the Alkaline Hydrogen Evolution Performance of Mo-Incorporated Ni(OH)2 by Plasma-Induced Heterostructure, Applied Catalysis B: Environmental 260 (2019) 118154. https://doi.org/10.1016/j.apcatb.2019.118154.

[14] P. Zhou, G. Zhai, X. Lv, Y. Liu, Z. Wang, P. Wang, Z. Zheng, H. Cheng, Y. Dai, B. Huang, Boosting the electrocatalytic HER performance of Ni3N-V2O3 via the interface coupling effect, Applied Catalysis B:

Environmental 283 (2021) 119590. https://doi.org/10.1016/j.apcatb.2020.119590.

[15] Q.-Q. Chen, X. Yang, C.-C. Hou, K. Li, Y. Chen, Inlay Ultrafine Ru Nanoparticles into Self-supported $Ni(OH)_2$ Nanoarry for Hydrogen Evolution with Low Overpotential and Enhanced Kinetics, Journal of Materials Chemistry A 7 (2019). https://doi.org/10.1039/C9TA02451D.

[16] X. Chen, Y. Lv, G. Zhang, Y. Huang, W. Liu, Y. Li, R. Chen, C. Nuckolls, H. Ni, An effective hybrid electrocatalyst for the alkaline HER: Highly dispersed Pt sites immobilized by a functionalized NiRu-hydroxide, Applied Catalysis B: Environmental 269 (2020) 118824. https://doi.org/10.1016/j.apcatb.2020.118824.

[17] Q. He, D. Tian, H. Jiang, D. Cao, S. Wei, D. Liu, P. Song, Y. Lin, L. Song, Achieving Efficient Alkaline Hydrogen Evolution Reaction over a Ni5P4 Catalyst Incorporating Single-Atomic Ru Sites, Advanced Materials 32 (2020). https://doi.org/10.1002/adma.201906972.

[18] J. Su, Y. Yang, G. Xia, J. Chen, P. Jiang, Q. Chen, Ruthenium-Cobalt Nanoalloys Encapsulated in Nitrogen-Doped Graphene as Active Electrocatalysts for Producing Hydrogen in Alkaline Media, Nature Communications 8 (2017) 14969. https://doi.org/10.1038/ncomms14969.

[19] Y. Liu, Y. Yang, Z. Liu, Z. Chen, L. Shang, S. Lu, T. Zhang, Self-crosslinking carbon dots loaded ruthenium dots as an efficient and super-stable hydrogen production electrocatalyst at all pH values, Nano Energy 65 (2019) 104023. https://doi.org/10.1016/j.nanoen.2019.104023.

[20] G. Chen, T. Wang, J. Zhang, P. Liu, H. Sun, X. Zhuang, M. Chen, X. Feng, Accelerated Hydrogen Evolution Kinetics on NiFe-Layered Double Hydroxide Electrocatalysts by Tailoring Water Dissociation Active Sites, Advanced Materials 30 (2018). https://doi.org/10.1002/adma.201706279.

[21] L. Bai, Z. Duan, X. Wen, R. Si, Q. Zhang, J. Guan, Highly Dispersed Ruthenium-Based Multifunctional Electrocatalyst, ACS Catalysis 2019 (2019). https://doi.org/10.1021/acscatal.9b03514.

[22] Z. Xing, C. Han, D. Wang, Q. Li, X. Yang, Ultrafine Pt Nanoparticle-Decorated Co(OH) 2 Nanosheet Arrays with Enhanced Catalytic Activity toward Hydrogen Evolution, ACS Catalysis 7 (2017) 7131-7135. https://doi.org/10.1021/acscatal.7b01994.

[23] Q. Wang, H. Xu, X. Qian, G. He, H. Chen, Sulfur vacancies engineered self-supported Co3S4 nanoflowers as an efficient bifunctional catalyst for electrochemical water splitting, Applied Catalysis B: Environmental 322 (2022) 122104. https://doi.org/10.1016/j.apcatb.2022.122104.

[24] Y. Liu, H. Zhang, Y. Zhang, W. Song, Z. Hou, G. Zhou, Z. Zhang, J. Liu, In-situ Growth of ReS2/NiS Heterostructure on Ni Foam as an Ultra-stable Electrocatalyst for Alkaline Hydrogen Generation, Chemical Engineering Journal 451 (2022) 138905. https://doi.org/10.1016/j.cej.2022.138905.

[25] Q.Q. Sun, Y.J. Dong, Z.L. Wang, S.W. Yin, C. Zhao, Synergistic Nanotubular Copper-Doped Nickel Catalysts for Hydrogen Evolution Reactions, Small 14(14) (2018) 1704137. https://doi.org/10.1002/smll.201704137.

[26] K.L. Zhou, Z. Wang, C.B. Han, X. Ke, C. Wang, Y. Jin, Q. Zhang, J. Liu, H. Wang, H. Yan, Platinum single-atom catalyst coupled with transition metal/metal oxide heterostructure for accelerating alkaline hydrogen evolution reaction, Nature Communications 12(1) (2021) 3783. https://doi.org/10.1038/s41467-021-24079-8.